A Calibration Technique for a Redundant IMU Containing Low-Grade Inertial Sensors

Seong Yun Cho and Chan Gook Park

A calibration technique for a redundant inertial measurement unit (IMU) containing low-grade inertial sensors is proposed. In order to calibrate a redundant IMU that can detect and isolate faulty sensors, the fundamental coordinate frames in the IMU are defined and the IMU error is modeled based on the frames. Equations to estimate the error coefficients of the redundant IMU are formulated, and a test sequence using a 2-axis turntable is also presented. Finally, a redundant IMU with cone configuration is implemented using low-grade inertial sensors, and the performance of the proposed technique is verified experimentally.

Keywords: Calibration, cone configuration redundant IMU, rate test, multi-position test.

I. Introduction

An inertial measurement unit (IMU) is a sensor assembly constructed by inertial sensors such as accelerometers and gyros. An IMU can measure the linear acceleration and angular velocity of a vehicle to calculate its navigational information, and is the core equipment in an inertial navigation system [1], [2]. An ordinary IMU consists of three accelerometers and three gyros. In general, the sensors in an ordinary IMU have an orthogonal configuration. Therefore, this IMU cannot detect the faults of the sensors. In this case, the navigation system may have an enormous error due to these faults. In order to overcome this problem, research on the redundant IMU (RIMU), which has a redundant sensor configuration and can detect and isolate faults, has been carried out [3]-[5]. The RIMU is indispensable in systems that require high reliability such as airplanes, launch vehicles, satellites, and so on.

So far, the research on optimal sensor configurations and fault detection techniques has been carried out mainly because the fault detection performance and navigation efficiency of an RIMU vary according to the sensor configurations. In order to maximize the fault detectable number, various sensor configurations have been researched, and a condition for optimal configuration of the six sensors was presented by Gilmore [3]. There are various sensor configurations such as symmetric, cone, orthogonal, and others. In these configurations, the cone configuration has the best fault detection and isolation (FDI) performance [5]. And fault detection techniques such as the parity space approach, generalized likelihood ratio test, state χ^2 test, and others have been investigated [4]-[6]. In FDI, it is assumed that the sensor inherent errors are already compensated. *Calibration* is used to evaluate the coefficients of the sensor errors in order to

Manuscript received Dec. 15, 2004; revised Mar. 15, 2005.

Seong Yun Cho (phone : +82 42 860 5847, email : sycho@etri.re.kr) is with Telematics Research Division, ETRI, Daejeon, Korea.

Chan Gook Park (email : chanpark@snu.ac.kr) is with the School of Mechanical and Aerospace Engineering and the Institute of Advanced Aerospace Technology, Seoul National University, Seoul, Korea.

compensate for them. This must be carried out before using the IMU. However, the research on the efficient calibration techniques for the RIMU is currently insufficient. Successful research on a conventional calibration technique for an orthogonal IMU has been carried out since 1970. First, the error models were designed. Then, the estimation techniques of the error coefficients were presented. In order to obtain the proper sensor outputs for calibration, a 2-or 3-axis turntable was used [9]-[12]. Recently, a calibration technique for the misalignment of the RIMU has been investigated [13], [14].

In this paper, a calibration technique for the RIMU is proposed. It is assumed that the RIMU is constructed by combining two tilted 6-DOF (degree of freedom) orthogonal IMUs to obtain a cone configuration easily. And the inertial sensors used in the IMU are the low-grade MEMS type. First, IMU internal coordinate frames such as a body frame fixed on the IMU case and the body frames fixed on the sub IMUs are defined. These frames can be utilized in every redundant sensor configuration. The IMU errors such as bias, misalignment, and scale factor error are expressed in these frames. Then, the error model equation is rearranged to apply the least square technique. In order to estimate the error coefficients, the proper sensor data that satisfies the observability of the measurement equation is necessary. Finally, a calibration procedure of the 2-axis turntable for the cone configuration IMU is proposed. The performance of the proposed calibration technique is also verified by experiment for the RIMU containing a cone configuration, and the error coefficients of the implemented IMU are successfully estimated.

This paper is organized into six sections. In section II, error modeling for the RIMU is carried out. Then, the error coefficients are estimated using equation rearranging and the least square technique in section III. In section IV, a calibration procedure of the 2-axis turntable for the cone configuration IMU is proposed. Next, the performance of the proposed technique is verified experimentally in section V. Finally, conclusions are drawn in the last section.

II. Error Modeling

In order to calibrate an RIMU, an error model must be designed. The RIMU has complex and various structures according to the sensor configurations. To design the error model for the RIMU regardless of the sensor configurations, fundamental coordinate frames of the RIMU must be defined first. Then, the error model is designed based on the coordinate frames. Certainly, an exact definition of the coordinate frames is the cornerstone for the error compensation of the RIMU. In this paper, it is assumed that the RIMU is implemented by combining the tilted two sensor modules or two orthogonal IMUs. The following three coordinate frames are defined for the calibration of the RIMU.

- Master Body (MB) frame : x_m, y_m, z_m
- Sub Body ^{j} (SB^j) frame : x_s^j, y_s^j, z_s^j
- Calculated Sub Body ^{j} (CSB^j) frame : $x_{cs}^j, y_{cs}^j, z_{cs}^j$

The relations between the frames are shown in Fig. 1. Here, the MS frame is the fixed frame on the outer case of the RIMU, and the three axes are orthogonal. In general, this frame corresponds to the body frame of a vehicle when the RIMU is attached on the vehicle. The SB^j frame is the body frame of the *j*-th sub IMU that is comprised in the RIMU. It is assumed that the angle between the MB frame and SB^j frame is rigidly fixed. And the angle can be represented as a direction cosine matrix (DCM). The CSB^j frame is the calculated SB^j frame using the MB frame and the DCM. In an ideal case, the SB^j frame and CSB^j frame must be identified. However, a misalignment error between the two frames exists as shown in Fig. 1. Before using the RIMU, the sensor level and system level errors such as misalignment error, bias, scale factor, and so on must be compensated for. In this paper, it is assumed that the inertial sensors used in the RIMU are low-grade MEMS sensors. Therefore, the error model is designed as in (1) by considering just 3 error factors: misalignment error, bias, and scale factor.

$$\begin{bmatrix} SF_x^1 \cdot x_s^1 \\ SF_y^1 \cdot y_s^1 \\ SF_z^1 \cdot z_s^1 \\ \hdashline SF_x^2 \cdot x_s^2 \\ SF_y^2 \cdot y_s^2 \\ SF_z^2 \cdot z_s^2 \end{bmatrix} = \begin{bmatrix} m_{xx}^1 & m_{xy}^1 & m_{xz}^1 & \multicolumn{3}{c}{\multirow{3}{*}{$0_{3\times3}$}} \\ m_{yx}^1 & m_{yy}^1 & m_{yz}^1 & \multicolumn{3}{c}{} \\ m_{zx}^1 & m_{zy}^1 & m_{zz}^1 & \multicolumn{3}{c}{} \\ \hdashline \multicolumn{3}{c}{\multirow{3}{*}{$0_{3\times3}$}} & m_{xx}^2 & m_{xy}^2 & m_{xz}^2 \\ \multicolumn{3}{c}{} & m_{yx}^2 & m_{yy}^2 & m_{yz}^2 \\ \multicolumn{3}{c}{} & m_{zx}^2 & m_{zy}^2 & m_{zz}^2 \end{bmatrix} \times \begin{bmatrix} h_{xx}^1 & h_{xy}^1 & h_{xz}^1 \\ h_{yx}^1 & h_{yy}^1 & h_{yz}^1 \\ h_{zx}^1 & h_{zy}^1 & h_{zz}^1 \\ \hdashline h_{xx}^2 & h_{xy}^2 & h_{xz}^2 \\ h_{yx}^2 & h_{yy}^2 & h_{yz}^2 \\ h_{zx}^2 & h_{zy}^2 & h_{zz}^2 \end{bmatrix} \begin{bmatrix} x_m \\ y_m \\ z_m \end{bmatrix} + \begin{bmatrix} b_x^1 \\ b_y^1 \\ b_z^1 \\ \hdashline b_x^2 \\ b_y^2 \\ b_z^2 \end{bmatrix} + \begin{bmatrix} v_x^1 \\ v_y^1 \\ v_z^1 \\ \hdashline v_x^2 \\ v_y^2 \\ v_z^2 \end{bmatrix}$$

$$\text{or} \quad Y = M \cdot H \cdot X + B + V \,, \tag{1}$$

where H is the DCM, M the misalignment error between the CSB frame and SB frame, B the sensor bias, and SF the scale factor of the sensor output. Also, i_s^j indicates the *i*-axis sensor output in the *j*-th sub-IMU and V denotes the white noise. The misalignment error is represented as follows:

$$\begin{aligned} \cos\alpha &= m_{xx}^j, \\ \cos\beta &= m_{xy}^j, \\ \cos\gamma &= m_{xz}^j \,. \end{aligned} \tag{2}$$

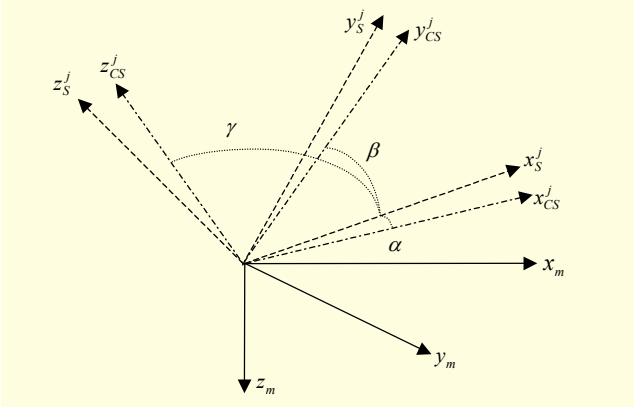

Fig. 1. Coordinate definition for the redundant IMU.

The misalignment error between sub-IMUs is not considered because it is assumed that the sub-IMUs are mounted on the case of the master body, independently. An estimation technique for the error coefficients in (1) is explained in the next section.

III. Estimation of the Error Coefficients

Equation (1) can be utilized in modeling the errors of both the accelerometer and gyro assemblies. The error coefficients of accelerometer assemblies can be estimated using only a multi-position test, while those of gyro assemblies can be estimated using the rate test and multi-position test. In the multi-position test, the outputs of gyros and accelerometers are examined at the various stationary positions. And the outputs of gyros on the turntable, rotated with constant angular velocity, are utilized in a rate test.

For estimating each error coefficient of the RIMU according to each axis, (1) is rearranged to apply the least square technique.

1. Calibration of the Accelerometer Assemblies

In (1), the equation for the i-axis accelerometer of j-th sub-IMU is represented as (3).

$$SF_i^j \cdot i_s^j = \begin{bmatrix} m_{ix}^j & m_{iy}^j & m_{iz}^j \end{bmatrix} \begin{bmatrix} h_{xx}^j & h_{xy}^j & h_{xz}^j \\ h_{yx}^j & h_{yy}^j & h_{yz}^j \\ h_{zx}^j & h_{zy}^j & h_{zz}^j \end{bmatrix} \begin{bmatrix} x_m \\ y_m \\ z_m \end{bmatrix} + b_i^j + v_i^j \quad (3)$$

In order to estimate the error coefficients in (3) using the least square technique, (3) is described by a linear equation of the form

$$Y = CX \,, \quad (4)$$

where Y is the sensor output, and X is the error coefficients to be estimated.

Equation (3) is rearranged as the following linear equation:

$$i_s^j = \begin{bmatrix} s_x^j & s_y^j & s_z^j & 1 \end{bmatrix} \begin{bmatrix} m_{ix}^j / SF_i^j \\ m_{iy}^j / SF_i^j \\ m_{iz}^j / SF_i^j \\ b_i^j / SF_i^j \end{bmatrix} + v_i^j \,, \quad (5)$$

where $i = x, y, z$, $j = 1, 2,$ and

$$\begin{bmatrix} s_x^j \\ s_y^j \\ s_z^j \end{bmatrix} = \begin{bmatrix} h_{xx}^j & h_{xy}^j & h_{xz}^j \\ h_{yx}^j & h_{yy}^j & h_{yz}^j \\ h_{zx}^j & h_{zy}^j & h_{zz}^j \end{bmatrix} \begin{bmatrix} x_m \\ y_m \\ z_m \end{bmatrix}. \quad (6)$$

Equation (6) is a known value when the position of the turntable is known and stationary. After saving the outputs of accelerometers at the known stationary positions, the error coefficients in (4) can be estimated using the least square technique as follows:

$$\begin{bmatrix} m_{ix}^j / SF_i^j \\ m_{iy}^j / SF_i^j \\ m_{iz}^j / SF_i^j \\ b_i^j / SF_i^j \end{bmatrix} = \left((S^j)^T S^j \right)^{-1} (S^j)^T Y_a^j \,, \quad (7)$$

where

$$S^j = \begin{bmatrix} s_x^j(1) & s_y^j(1) & s_z^j(1) & 1 \\ \vdots & \vdots & \vdots & \vdots \\ s_x^j(n) & s_y^j(n) & s_z^j(n) & 1 \end{bmatrix}, \text{ and} \quad (8)$$

$$Y_a^j = \begin{bmatrix} \bar{i}_s^j(1) & \bar{i}_s^j(2) & \cdots & \bar{i}_s^j(n) \end{bmatrix}^T \quad (9)$$

for every $n \geq 4$. The value of S is known, Y is the mean value of the output of the i-axis accelerometer in j-th sub-IMU, and n is the number of positions in a multi-position test.

In order to estimate the error coefficients in (7), the following DCM constraint is also necessary.

$$\left(m_{ix}^j\right)^2 + \left(m_{iy}^j\right)^2 + \left(m_{iz}^j\right)^2 = 1 \quad (10)$$

First, the scale factor is estimated using (7) and (10). Then, the misalignment error and bias are estimated using (7) and the estimated scale factor.

2. Calibration of the Gyro Assemblies

In order to estimate the misalignment errors and the scale factors of gyro assemblies, a rate test is required. Also, a multi-

position test is used to estimate the biases. At the *k*-th step, the particular axis of the turntable is rotated with angular velocity ω. At the (*k*+1)th step, the axis of the turntable rotated at the *k*-th step is turned with angular velocity $-\omega$. Then, the equation for the *i*-axis gyro of the *j*-th sub-IMU is represented as follows:

$$i_s^j(k) - i_s^j(k-1) = \begin{bmatrix} r_x^j & r_y^j & r_z^j \end{bmatrix} \begin{bmatrix} m_{ix}^j / SF_i^j \\ m_{iy}^j / SF_i^j \\ m_{iz}^j / SF_i^j \end{bmatrix} + v, \quad (11)$$

where

$$\begin{bmatrix} r_x^j \\ r_y^j \\ r_z^j \end{bmatrix} = \begin{bmatrix} h_{xx}^j & h_{xy}^j & h_{xz}^j \\ h_{yx}^j & h_{yy}^j & h_{yz}^j \\ h_{zx}^j & h_{zy}^j & h_{zz}^j \end{bmatrix} \begin{bmatrix} x_m(k) - x_m(k+1) \\ y_m(k) - y_m(k+1) \\ z_m(k) - z_m(k+1) \end{bmatrix}. \quad (12)$$

Equation (12) is a known value when the angular velocity of the turntable is known. After saving the outputs of the gyros in the rate test, the misalignment errors and the scale factors of the gyros are estimated using the least square technique.

$$\begin{bmatrix} m_{ix}^j / SF_i^j \\ m_{iy}^j / SF_i^j \\ m_{iz}^j / SF_i^j \end{bmatrix} = \left((R^j)^T R^j \right)^{-1} (R^j)^T Y_g^j, \quad (13)$$

where

$$R^j = \begin{bmatrix} r_x^j(1) & r_y^j(1) & r_z^j(1) \\ \vdots & \vdots & \vdots \\ r_x^j(n) & r_y^j(n) & r_z^j(n) \end{bmatrix}, \text{ and} \quad (14)$$

$$Y_g^j = \begin{bmatrix} \bar{i}_s^j(1) - \bar{i}_s^j(2) \\ \bar{i}_s^j(3) - \bar{i}_s^j(4) \\ \vdots \\ \bar{i}_s^j(2n-1) - \bar{i}_s^j(2n) \end{bmatrix} \quad (15)$$

for every $n \geq 3$. Value $\bar{i}_s^j(k)$ indicates the mean value of the gyro output during the rate test at the *k*-th step.

In the multi-position test for gyros, the gyro biases are represented as

$$b_i^j = SF_i^j \cdot i_s^j. \quad (16)$$

After saving the outputs of the gyros in the multi-position test, the gyro biases are estimated as follows:

$$b_i^j = SF_i^j \cdot \frac{1}{n} \sum_{k=1}^{n} i_s^j(k) \quad (17)$$

for every $n \geq 1$.

IV. Test Procedure of the 2-axis Turntable for the Cone Configuration IMU

An RIMU can be implemented with a symmetric configuration, cone configuration, orthogonal configuration, and so on. In these configurations, the orthogonal-cone configuration as shown in Fig. 2 has the best FDI performance. In this figure, $\overline{o_m i_s^j}$ makes a right angle with $\overline{o_m k_s^j}$, where *i*, *k*=*x*, *y* and z, $i \neq k$. Also, $\angle i_s^j o_m(-z_m) = 54.7356^\circ$. Therefore, the orthogonal-cone configuration has the following DCM.

$$H = \begin{bmatrix} \frac{\sqrt{2}}{\sqrt{3}} & 0 & -\frac{1}{\sqrt{3}} \\ -\frac{1}{\sqrt{6}} & -\frac{1}{\sqrt{2}} & -\frac{1}{\sqrt{3}} \\ -\frac{1}{\sqrt{6}} & \frac{1}{\sqrt{2}} & -\frac{1}{\sqrt{3}} \\ -\frac{\sqrt{2}}{\sqrt{3}} & 0 & -\frac{1}{\sqrt{3}} \\ \frac{1}{\sqrt{6}} & \frac{1}{\sqrt{2}} & -\frac{1}{\sqrt{3}} \\ \frac{1}{\sqrt{6}} & -\frac{1}{\sqrt{2}} & -\frac{1}{\sqrt{3}} \end{bmatrix}. \quad (18)$$

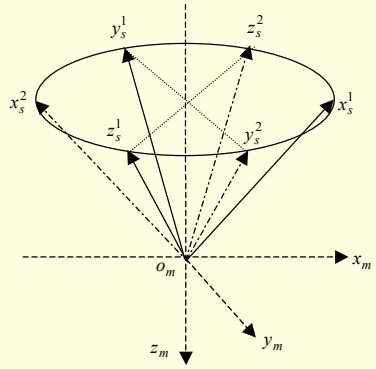

(a) Sensor configuration

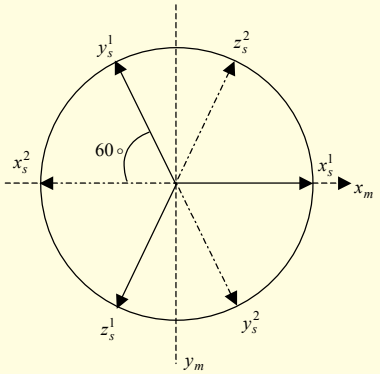

(b) Cross-sectional view

Fig. 2. Orthogonal-cone configuration IMU.

The sensor data required for estimating the error coefficients is obtained using the turntable. In order to obtain the proper sensor data, a test procedure for the turntable is designed. Using the test procedure, a rate test and multi-position test are carried out.

The test procedure for the turntable may be designed according to the turntable structure and the sensor configuration of the RIMU. In this section, a test procedure of the 2-axis turntable for the cone configuration IMU is designed. The 2-axis turntable consists of a table axis and tilt axis. The tilt axis is aligned with the North and the table axis is aligned with Up. The IMU is attached on the table. The z-axis of the MB frame is aligned with the table axis, and the x-axis of the MB frame is aligned with the tilt axis. Then, the rate table is operated according to the procedure denoted in Tables 1 and 2.

Table 1. Multi-position test procedure.

Sequence	Input acceleration		
	x_m	y_m	z_m
1	0	0	$-g$
2	0	$-g$	0
3	0	0	g
4	0	g	0
5	g	0	0
6	$-g$	0	0
7	$-g\cos 45°$	$g\sin 45°$	0
8	$g\cos 45°$	$g\sin 45°$	0
9	$-g\cos 45°$	0	$g\sin 45°$
10	$g\cos 45°$	0	$g\sin 45°$

Table 2. Rate test procedure.

Sequence	Input acceleration		
	x_m	y_m	z_m
1	ω_{rt}	0	0
2	$-\omega_{rt}$	0	0
3	0	ω_{rt}	0
4	0	$-\omega_{rt}$	0
5	0	0	ω_{rt}
6	0	0	$-\omega_{rt}$
7	$-\omega_{rt}\sin 30°$	$-\omega_{rt}\cos 30°$	0
8	$\omega_{rt}\sin 30°$	$\omega_{rt}\cos 30°$	0
9	$-\omega_{rt}\sin 30°$	$\omega_{rt}\cos 30°$	0
10	$\omega_{rt}\sin 30°$	$-\omega_{rt}\cos 30°$	0
11	$\omega_{rt}\sin 45$	$-\omega_{rt}\cos 45°$	0
12	$-\omega_{rt}\sin 45°$	$\omega_{rt}\cos 45°$	0
13	$\omega_{rt}\sin 45°$	$\omega_{rt}\cos 45°$	0
14	$-\omega_{rt}\sin 45°$	$-\omega_{rt}\cos 45°$	0

In order to decide on the number of test procedure sequences, the standard deviation of error is utilized. The diagonal terms of (19a) for the multi-position test and (19b) for the rate test are analyzed.

$$\left((S^j)^T S^j\right)^{-1} \tag{19a}$$

$$\left((R^j)^T R^j\right)^{-1} \tag{19b}$$

Figure 3 shows the standard deviations of the misalignment error and bias according to the number of test procedure sequences denoted in Tables 1 and 2. As can be seen in this figure, the larger the number of the test procedure sequence, the less the standard deviation of the estimation error. Therefore, the estimation error can be reduced by setting the test procedure variously. However, it is necessary to set the test procedure properly in consideration of the test time.

In this paper, the number of the test procedure sequence for the rate test is set as 10 and that for the multi-position test is set as 6 because the decreasing rate of the estimation error is gradually reduced at this point.

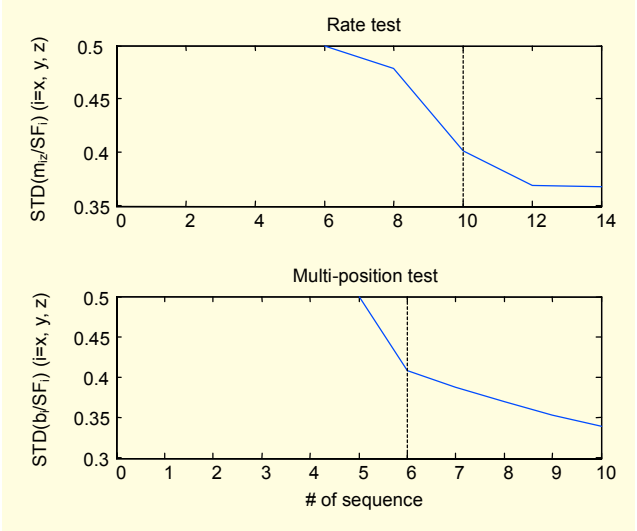

Fig. 3. Standard deviation of the estimation error according to the number of the test procedure sequence.

V. Experimental Results

In order to analyze the performance of the proposed calibration technique for the RIMU, a cone configuration IMU is implemented. Two orthogonal IMUs are combined to

construct the cone configuration as can be seen in Fig. 4. The sensor configuration in the IMU is identical with Fig. 2.

The system block diagram of the implemented RIMU is denoted in Fig. 4(b). The two orthogonal IMUs individually have 6-DOF with three accelerometers and three gyros. The sensors used are MEMS-type low-cost sensors (accelerometer: ADXL202E, gyro: ADXRS150). The sensor outputs are digitized using a microcontroller. Data transmission between the two IMUs is performed using a SPI (serial peripheral interface) that allows for a high-speed synchronous data transfer. The digitized sensor outputs of the two IMUs are gathered in one microcontroller and are transferred to a navigation computer through a UART (universal asynchronous serial receiver and transmitter).

The implemented RIMU is mounted on the 2-axis turntable (ACT-2000). ACT-2000 has an attitude error of less than 10^{-4} degrees and an angular velocity error of less than 10^{-3} deg/sec. The turntable is operated according to the test procedure denoted in Tables 1 and 2. During the test, the sensor data is saved in the memory of the navigation computer. Then, the error coefficients of the implemented RIMU are estimated using the proposed calibration technique.

The estimated error coefficients are represented in Table 3. As can be seen in this table, the misalignment error is not a negligible quantity, and it occurred during implementation.

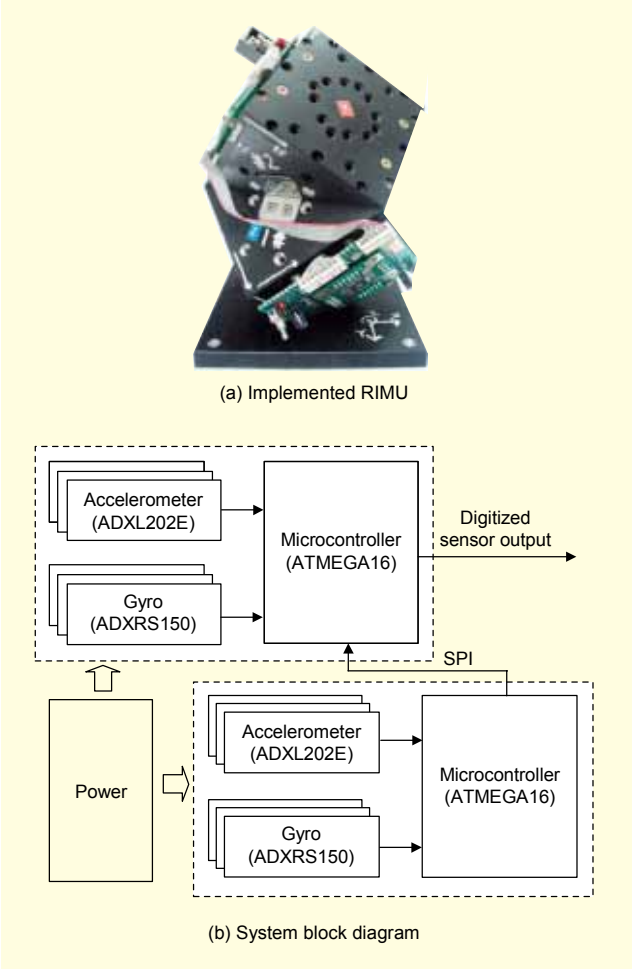

Fig. 4. Implemented RIMU with cone configuration.

Table 3. Estimated error coefficients.

Gyro			
Sub-IMU 1		Sub-IMU 2	
Coef.	Value	Coef.	Value
SF_x^1	3.8228e-1	SF_x^2	3.8673e-1
SF_y^1	3.9791e-1	SF_y^2	3.9207e-1
SF_z^1	3.8469e-1	SF_z^2	3.8685e-1
b_x^1	1.9091e+2	b_x^2	1.8354e+2
b_y^1	2.0820e+2	b_y^2	1.9367e+2
b_z^1	1.9168e+2	b_z^2	1.8348e+2
m_{xx}^1	9.9981e-1	m_{xx}^2	9.9957e-1
m_{xy}^1	-1.8872e-1	m_{xy}^2	-2.7609e-2
m_{xz}^1	-3.9341e-3	m_{xz}^2	-9.7901e-3
m_{yx}^1	-6.8270e-3	m_{yx}^2	-6.5264e-3
m_{yy}^1	9.9997e-1	m_{yy}^2	9.9994e-1
m_{yz}^1	3.6380e-3	m_{yz}^2	-7.9822e-3
m_{zx}^1	-8.5066e-5	m_{zx}^2	-5.9459e-3
m_{zy}^1	-1.7047e-3	m_{zy}^2	-1.0184e-2
m_{zz}^1	9.9999e-1	m_{zz}^2	9.9993e-1
Accelerometer			
Sub-IMU 1		Sub-IMU 2	
Coef.	Value	Coef.	Value
SF_x^1	2.2498e-4	SF_x^2	1.8836e-4
SF_y^1	2.1681e-4	SF_y^2	1.8858e-4
SF_z^1	2.3295e-4	SF_z^2	2.5085e-4
b_x^1	3.6463	b_x^2	3.9279
b_y^1	4.0643	b_y^2	3.2673
b_z^1	4.1861	b_z^2	3.5403
m_{xx}^1	9.9959e-1	m_{xx}^2	9.9984e-1
m_{xy}^1	2.2858e-2	m_{xy}^2	1.2791e-2
m_{xz}^1	-1.6705e-2	m_{xz}^2	-1.2181e-2
m_{yx}^1	1.0886e-2	m_{yx}^2	-1.4933e-2
m_{yy}^1	9.9993e-1	m_{yy}^2	9.9966e-1
$m_{yz}^1 o$	4.4292e-3	m_{yz}^2	2.1193e-2
m_{zx}^1	1.3533e-2	m_{zx}^2	-2.3119e-3
m_{zy}^1	-3.6061e-3	m_{zy}^2	5.6244e-4
m_{zz}^1	9.9990e-1	m_{zz}^2	9.9999e-1

Therefore, calibration must be processed before using the implemented RIMU. After calibration, the sensor data in the master body frame is calculated by the use of

$$\begin{bmatrix} \hat{x}_m & \hat{y}_m & \hat{z}_m \end{bmatrix}^T = \left(H^T H\right)^{-1} H^T M^{-1} \left(Y - B\right). \quad (20)$$

Table 4. Error performance after calibration.

	Gyro (°/s)		Accelerometer (g)	
	Mean	S. D.	Mean	S. D.
X-axis	-3.0013e-2	3.5272e-1	4.6999e-4	1.0650e-3
Y-axis	1.9621e-2	3.3129e-1	1.9599e-4	1.0390e-3
Z-axis	-6.7242e-2	3.2640e-1	4.7600e-4	1.0649e-3

g: gravity

The result after calibration is shown in Fig. 5. Figure 5(a) shows the angular velocity when the RIMU is rotated 30 [deg/sec] along the y-axis. And Fig. 4(b) represents the acceleration detected in the master body frame when the position of the RIMU is NUE (North, Up and East).

As you can see in Fig. 5, the calibration process is accomplished very well. Table 4 shows the error performance after calibration. The performance of the gyros indicates the maximum mean values among 14 cases given in Table 1, and that of the accelerometers is the maximum mean value among 10 positions denoted in Table 2. It can be seen that the errors of the gyros are less than 7.5e-2 °/s and those of the accelerometers are less than 5.0e-4 g. Therefore, the performance of the RIMU after calibration is reasonable. And the performance of the proposed calibration technique is verified by our experiments.

An RIMU can be utilized continuously even when a sensor

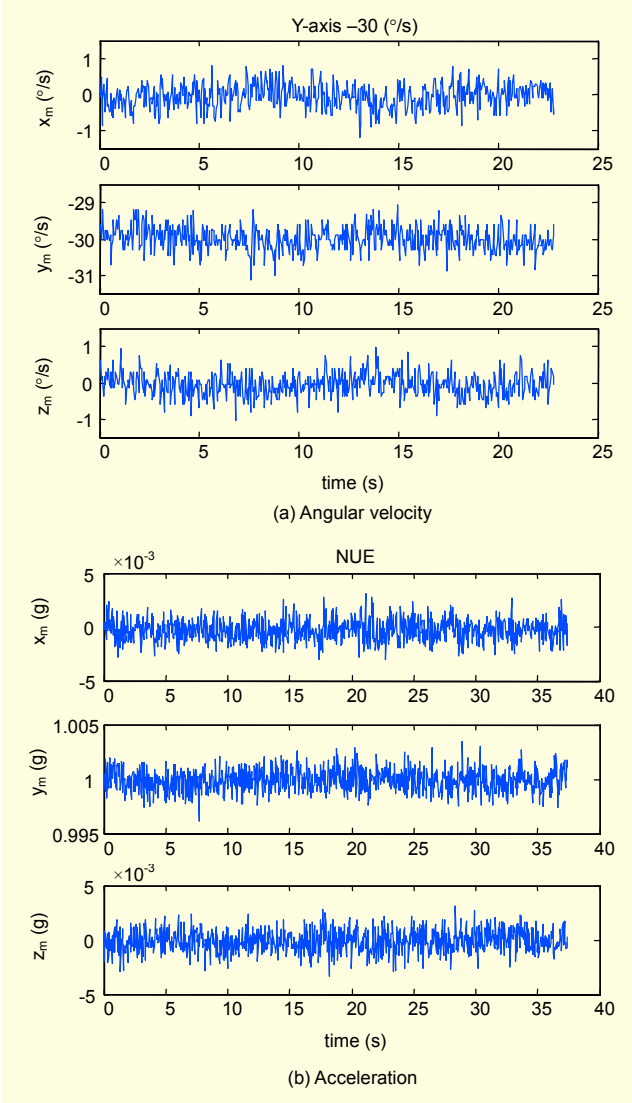

Fig. 5. Results after calibration.

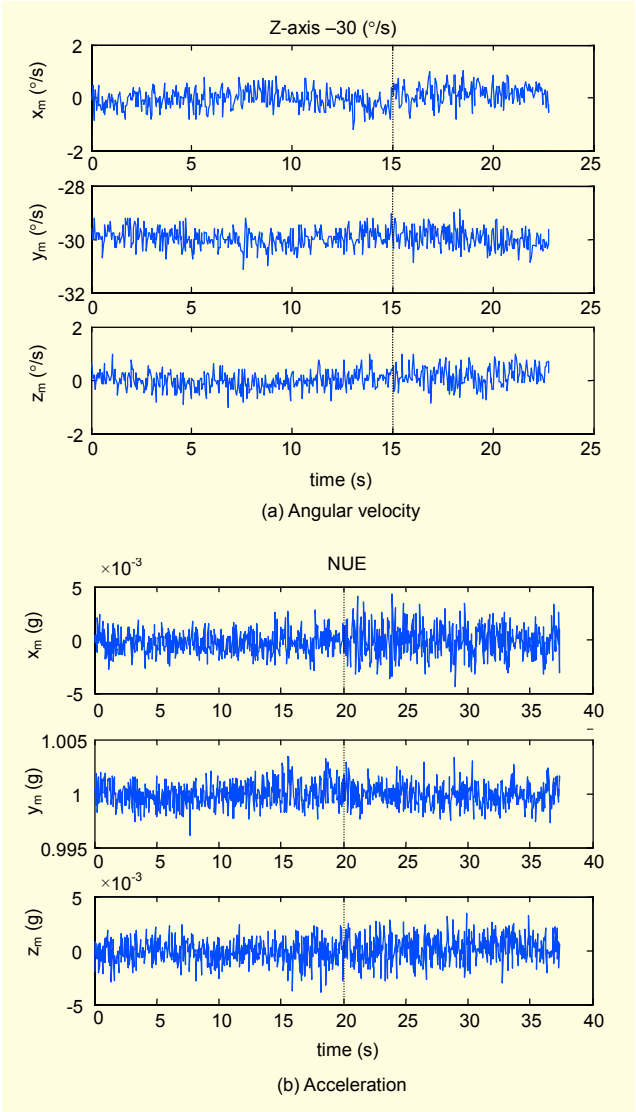

Fig. 6. Results after fault occurrence.

fault occurs because of the sensor redundancy. Figure 6 denotes the sensor output along the MB frame before and after fault occurrence. The fault configuration is as follows:

- Y-axis gyro (y_s^2) has a fault after 15 seconds.
- X-axis accelerometer (x_s^1) has a fault after 20 seconds.

It is assumed that the fault can be detected using a proper algorithm. When a fault is detected in the y-axis sensor of sub-IMU 2, the fault can be isolated by setting the corresponding parameters as follows:

$$y_s^2 = 0\,,\quad b_y^2 = 0\,,\text{ and }\quad H = \begin{bmatrix} h_{xx}^1 & h_{xy}^1 & h_{xz}^1 \\ h_{yx}^1 & h_{yy}^1 & h_{yz}^1 \\ h_{zx}^1 & h_{zy}^1 & h_{zz}^1 \\ \hdashline h_{xx}^2 & h_{xy}^2 & h_{xz}^2 \\ 0 & 0 & 0 \\ h_{zx}^2 & h_{zy}^2 & h_{zz}^2 \end{bmatrix}. \qquad (21)$$

As can be seen in Fig. 6, the fault can be isolated successfully. The full dynamic information of the RIMU along the MB frame can be obtained after isolating the faulty sensor using (21). Table 5 denotes the standard deviation along the MB frame before and after a fault occurrence. As can be seen in this table, the standard deviation is slightly increased after isolating the faulty sensor. In this phenomenon, it can be seen that the sensor redundancy can reduce the standard deviation of the sensor noise. Moreover, the RIMU can be utilized normally even when the sensor fault has occurred.

Table 5. Standard deviation before and after fault occurrence.

	Gyro (°/s)		Accelerometer (g)	
	Before (0 –15s)	After (15s–)	Before (0 –20s)	After (20s–)
X-axis	3.4466e-1	3.5748e-1	9.8651e-4	1.4384e-3
Y-axis	3.4014e-1	3.7091e-1	1.1116e-3	1.0430e-3
Z-axis	3.1875e-1	3.8253e-1	1.0476e-3	1.2197e-3

g: gravity

VI. Conclusion

In this paper, a calibration technique for a redundant inertial measurement unit (RIMU) is proposed. The coordinate frames in the RIMU are defined, and the RIMU errors are modeled on the defined frames. The variables to be estimated are scale factor, misalignment error, and bias of the RIMU. In order to estimate these variables, the calibration equations and test procedure of the 2-axis turntable for the cone configuration RIMU are proposed. A cone configuration RIMU is also implemented for the performance verification of the proposed calibration technique. Then, the error coefficients of the implemented RIMU are estimated. The results show that the proposed calibration technique is very effective to calibrate the RIMU containing low-grade inertial sensors.

Reference

[1] Jay A. Farrell and Matthew Barth, *The Global Positioning System & Inertial Navigation*, McGraw-Hill, 1999.

[2] Seong-Baek Kim, et al., "A Bimodal Approach for Land Vehicle Localization," *ETRI J.*, vol. 26, no. 5, Oct. 2004, pp. 497-500.

[3] J. P. Gilmore, A Nonorthogonal Gyro Configuration, S.M. Thesis, Aeronautics and Astronautics Dept, M.I.T., Cambridge, MA, 1967.

[4] J. P. Gilmore, and R. A. Mckern, "A Redundant Strapdown Inertial Reference Unit (SIRU)," *J. Spacecraft*, vol. 9, no. 1, 1972.

[5] J. V. Harrison and E. G. Gai, "Evaluating Sensor Orientations for Navigation Performance and Failure Detection," *IEEE Trans Aerospace and Electronic Systems*, vol. 13, no. 6, 1977.

[6] J. E. Potter and M. C. Suman, "Thresholdless Redundancy Management with Arrays of Skewed Instruments," *Integrity in Electronic Flight Control Systems. NATO AGARDOGRAPH-224*, 1977.

[7] K. C. Daly, E. G. Gai, and J. V. Harrison, "Generalized Likelihood Test for FDI in Redundant Sensor Configurations," *AIAA J.*, vol. 2, no. 1, 1979.

[8] T. T. Chien and M. B. Adams, "A Sequential Failure Detection Technique and Its Application," *IEEE Trans Automatic Control*, 1976.

[9] U. Krogmann, "Identification Procedures for Strapdown Sensor Parameters by Laboratory Testing," *Symp. Gyro Technology*, 1978.

[10] D. K. Joos, "Determination and Evaluation of Strapdown-Sensor-Parameters from System-Test-Data," *Symp. Gyro Technology*, 1979.

[11] L. Camberlein and F. Mazzanti, "Calibration Technique for Laser Gyro Strap-down Inertial Navigation System," *Symp. Gyro Technology*, 1985.

[12] J. Mark, D. Tazartes, and T. Hilby, "Fast Orthogonal Calibration of a Ring Laser Strapdown System," *Symp. Gyro Technology*, 1986.

[13] Seong Yun Cho and Chan Gook Park, "Calibration of a Redundant IMU," *AIAA Guidance, Navigation and Control Conf. and Exhibit*, 2004.

[14] Mark E. Pittelkau, "RIMU Misalignment Vector Decomposition," *AIAA Guidance, Navigation and Control Conf. and Exhibit,* 2004.

Seong Yun Cho was born in Jinju, Korea, in 1974. He received the BS, MS, and PhD degrees in the Department of Control and Instrumentation Engineering from Kwangwoon University, Korea, in 1998, 2000, and 2004. In 2003, he was with the Automation and System Research Institute (ASRI), Seoul National University, Korea, where he worked on the development of a tilt compensation algorithm for a magnetic compass with Samsung Advanced Institute of Technology (SAIT) as a research assistant. In 2004, he was with the School of Mechanical and Aerospace Engineering, Seoul National University, Korea, where he was a postdoctoral fellow, BK21. Since 2004, he has been with Electronics and Telecommunications Research Institute (ETRI), Korea, as a Senior Member of Research Staff. His research interests include development of navigation systems (INS, INS/GPS, PNS), filter design for nonlinear systems, and development of telematics application systems.

Chan Gook Park was born in Seoul, Korea, in 1961. He received the BS, MS, and PhD degrees in control and instrumentation engineering from Seoul National University, Korea, in 1985, 1987, and 2003. He worked as a postdoctoral fellow at the Engineering Research Center for Advanced Control and Instrumentation, Seoul National University, in 1993. From 1994 to 2003, he was with Kwangwoon University, Korea, as an Associate Professor. In 2003, he joined the faculty of the School of Mechanical and Aerospace Engineering at Seoul National University, where he is currently an Associate Professor. In 1998, he was with Prof. Jason L. Speyer dealing with peak-seeking control for formation flight at University of California, Los Angeles (UCLA) as a visiting scholar. His research interests include filtering techniques, inertial navigation systems, GPS/INS integration, and personal navigation systems.